



SURVEY PERFORMANCE CALCULATIONS

Document number..... SKA-TEL-SKO-0000645
 Context..... SKA-OFFICE-SCI-SPC
 Revision.....01
 Author SKAO ST et al.
 Date..... 2016-09-06
 Document Classification UNRESTRICTED
 Status Released

Name	Designation	Affiliation	Signature	
Authored by:				
SKAO ST, Staveley-Smith, Johnston, Rathborne, p.p. Robert Braun	Science Director	SKAO		
			Date:	Sep 8, 2016
Owned by:				
Robert Braun	Science Director	SKAO		
			Date:	Sep 8, 2016
Approved by:				
Robert Braun	Science Director	SKAO		
			Date:	Sep 8, 2016
Released by:				
Alistair McPherson	Head of Project	SKAO		
			Date:	Sep 8, 2016

DOCUMENT HISTORY

Revision	Date Of Issue	Engineering Change Number	Comments
01	2016-09-06	-	First release of document

DOCUMENT SOFTWARE

	Package	Version	Filename
Word processor	MS Word	Word 2007	SKA-TEL-SKO-01-0000645-SurveyPerformance
Block diagrams			
Other			

ORGANISATION DETAILS

Name	SKA Organisation
Registered Address	Jodrell Bank Observatory Lower Withington Macclesfield Cheshire SK11 9DL United Kingdom Registered in England & Wales Company Number: 07881918
Fax.	+44 (0)161 306 9600
Website	www.skatelescope.org

TABLE OF CONTENTS

1	INTRODUCTION.....	6
1.1	Purpose of the document	6
1.2	Scope of the document.....	6
2	REFERENCES	7
2.1	Applicable documents.....	7
2.2	Reference documents.....	7
3	SURVEY SPEED PARAMETERS	8
3.1	Sensitivity of SKA1-MID.....	8
3.2	Sensitivity as function of angular scale for SKA1-MID	9
3.3	Field-of-View of SKA1-MID.....	10
3.4	Sensitivity of ASKAP	11
3.5	Sensitivity as function of angular scale for ASKAP	11
3.6	Field-of-View of ASKAP	12
3.7	Sensitivity and Field-of-View of PAFs on SKA1 dishes	12
4	SURVEY SPEED COMPARISONS.....	14
4.1	Relative Survey Speed of SKA1-MID and ASKAP MkII.....	14
4.2	Relative Survey Speed of SKA1-MID and ASKAP MkIII.....	15
4.3	Relative Survey Speed of SKA1 dishes with SPFs and PAFs	16

LIST OF FIGURES

Figure 1. The zenith sensitivity of each SKA1-MID dish. The blue curve shows estimated sensitivity in terms of the left hand axis labels, while the magenta curve shows the typical assumed sky temperature using the right hand axis labels. The dashed blue curve depicts bands not yet scheduled for deployment, while the frequency interval above 13.8 GHz is under investigation in the context of the Advanced Instrumentation Program (AIP).	8
Figure 2. Monochromatic (left) and broad-band (right) image noise and PSF quality performance of the SKA1-MID configuration as function of angular scale.	10
Figure 3. The ratio of system temperature to aperture efficiency T_{sys}/η_A of the ASKAP MkII PAF as published by Chippendale et al. in RD4.	11
Figure 4. Monochromatic (left) and broad-band (right) image noise of the ASKAP configuration as function of angular scale.	11
Figure 5. The number of noise effective ASKAP PAF beams as function of frequency as published by Hay et al. in RD5. The “oct36” label refers to the relevant octagonal arrangement of 188 differential ports sampled by 36 digital beams.	12
Figure 6. Overview of PAF performance within the SKA1 dish optics as function of frequency as published by Hay & Smith in RD6 assuming an LNA minimum differential noise temperature of 21K. The quantity SSFoM is defined as $\text{FoV} (\eta_A/T_{\text{sys}})^2$	13
Figure 7. Empirical model of PAF performance within the SKA1 dish optics as function of frequency (blue curves) overlaid on the performance simulations (black points) of Hay & Smith in RD6. The quantity SSFoM is defined as $\text{FoV} (\eta_A/T_{\text{sys}})^2$	14
Figure 8. The relative survey speed of SKA1-MID compared to ASKAP equipped with 36 MkII PAFs as function of observing frequency and Gaussian beam size. The ASKAP MkII sensitivity as function of frequency is taken from Chippendale et al [RD4]. The dashed horizontal line marks the boundary between SPF1 and SPF2 for SKA1.	15
Figure 9. The relative survey speed of SKA1-MID compared to ASKAP equipped with 36 MkIII PAFs as function of observing frequency and Gaussian beam size. The ASKAP MkIII sensitivity as assumed to be $T_{\text{sys}}/\eta \approx 50$ K over the full frequency range. The dashed horizontal line marks the boundary between SPF1 and SPF2 for SKA1.	16
Figure 10. The relative survey speed of SKA1 dishes when equipped with PAFs versus SPFs.	17

LIST OF ABBREVIATIONS

AIP	Advanced Instrumentation Programme
BD	SKA1 Baseline Design
DM.....	Dispersion Measure
EMI.....	Electromagnetic Interference
EoR	Epoch of Reionisation
FRB.....	Fast Radio Burst
FWHM.....	Full Width Half Maximum
HPSO.....	High Priority Science Objective
ISW	Integrated Sachs Wolfe effect
NIP	Non-image Processing
PAF	Phased Array Feed
PSF	Point Spread Function
RFI	Radio Frequency Interference
RM.....	Rotation Measure
RMS	Root Mean Square
SEFD.....	System Equivalent Flux Density
SKA.....	Square Kilometre Array
SKAO	SKA Organisation
SPF	Single Pixel Feed
VLBI	Very Long Baseline Interferometry

1 Introduction

1.1 Purpose of the document

This document is intended to provide an analysis of the relative survey speed performance of various antenna systems.

1.2 Scope of the document

A survey speed metric is defined and is subsequently evaluated and compared for several antenna systems. Systems that are currently contrasted are the ASKAP array, both as equipped with “MkII” PAF systems and with hypothetical upgraded “MkIII” PAF systems, as well as the planned SKA1-MID deployment both with SPFs and with hypothetical newly developed PAFs.

2 References

2.1 Applicable documents

The following documents are applicable to the extent stated herein. In the event of conflict between the contents of the applicable documents and this document, **the applicable documents** shall take precedence.

[AD1] SKA1 Level 1 Requirements

2.2 Reference documents

The following documents are referenced in this document. In the event of conflict between the contents of the referenced documents and this document, **this document** shall take precedence.

[RD1] SKA1 Level 0 Requirements

[RD2] Cortes, 2007, SKA memo 95

[RD3] Kraus, 1988, Antennas, p.856

[RD4] Chippendale et al. 2015, arXiv:1509.00544

[RD5] Hay et al. 2013, EuCAP2013, "FoV Analysis and Design for the ASKAP"

[RD6] Hay & Smith, 2014, SKA-TEL.DSH.SE-CSIRO-R-004, "PAF & Optics Electromagnetic Performance Analysis"

[RD7] Pantaleev et al. 2016, SKA-TEL-DSH-0000120-B, "SPF Band 1 Feed Package Selection"

[RD8] Peens-Hough et al. 2015, SKA-TEL.DSH.SE-NRF-R-003, "Summary of expected performance of the preferred dish optics for SKA"

[RD9] Condon et al. 2012, ApJ 758, 23, "Resolving the radio source background: deeper understanding through confusion"

3 Survey Speed Parameters

The most commonly used metric for Survey Speed (SS) is, $SS = (A_{\text{eff}}/T_{\text{sys}})^2 \times \text{FoV}$, the product of sensitivity (given by the effective aperture divided by the system temperature) squared with the noise effective Field-of-View, FoV. In some cases the SS definition is extended to include the processed bandwidth, BW, as $SS' = (A_{\text{eff}}/T_{\text{sys}})^2 \times \text{FoV} \times \text{BW}$, however this would only be appropriate for some scientific applications. We will utilise the more basic SS definition above, but will comment on differences in processed bandwidth where this is appropriate.

In the case of an interferometric array, the calculation of survey speed is further influenced by the array configuration. The simple formulation above would only apply to the interferometric beam that results from imaging all measured visibilities with their “natural” weights (that are proportional to the square of their intrinsic signal-to-noise ratio). When the array configuration spans a wide range of spatial scales with a radial distribution that is not inherently Gaussian, then the “natural” beam is rarely scientifically useful. It typically has an extremely non-Gaussian shape and a poorly defined flux scale. A more interesting metric for comparison is then the Survey Speed as function of the “most Gaussian possible” beam size. This is the quantity that we will consider below.

3.1 Sensitivity of SKA1-MID

Noise performance targets were given within the SKA1 Baseline Design for the Single Pixel Feeds (SPFs) of SKA1–MID. These have been superseded by the measurements of the actual preliminary designs as published in the PDR documentation [RD7 for SPF1 and RD8 for SPF2 – 5] that are now reflected in both the Level 0 [RD1] and Level 1 [AD1] requirements and shown for reference in Figure 1 below.

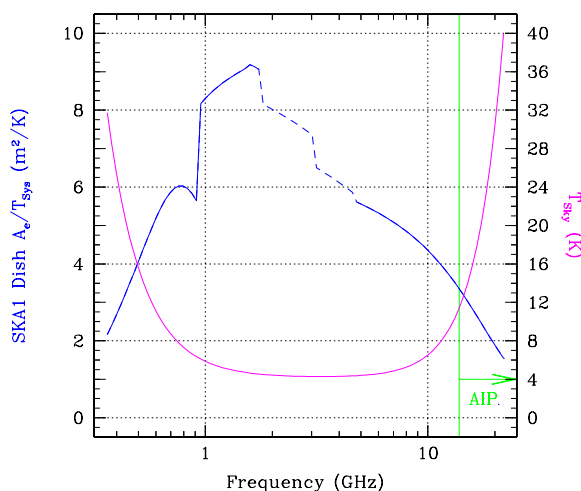


Figure 1. The zenith sensitivity of each SKA1-MID dish. The blue curve shows estimated sensitivity in terms of the left hand axis labels, while the magenta curve shows the typical assumed sky temperature using the right hand axis labels. The dashed blue curve depicts bands not yet scheduled for deployment, while the frequency interval above 13.8 GHz is under investigation in the context of the Advanced Instrumentation Program (AIP).

The model underlying the curves in Figure 1 has:

$$T_{\text{Sys}} = T_{\text{Rcvr}} + T_{\text{Spill}} + T_{\text{Sky}}, \text{ where}$$

$$T_{\text{Sky}} = T_{\text{Gal}} + T_{\text{CMB}} + T_{\text{Atm}} \text{ following [RD2] with,}$$

$$T_{\text{Gal}} = 20 (0.408 \text{ GHz}/\nu)^{2.75} \text{ K,}$$

$$T_{\text{CMB}} = 2.73 \text{ K and}$$

$$T_{\text{Atm}} = 288 (0.005 + 0.1314 \exp\{8[\log_{10}(\nu) - \log_{10}(22.23 \text{ GHz})]\}) \text{ K}$$

where the atmospheric contribution is only being modelled up to the water line at 22.23 GHz. The spill-over component, T_{Spill} , is modelled as a constant, $T_{\text{Spill}} = 4$ K for simplicity.

Current estimates of T_{Rcvr} for each of the SKA1 SPF bands and their variation with the frequency in GHz, ν , are given by:

$$\begin{aligned} \text{SKA SPF1 (350 – 1050 MHz): } T_{\text{Rcvr}} &= 11.5 + 8.0[(\nu-0.65)/(1.05-0.35)]^2 \text{ K} \\ \text{SKA SPF2 (950 – 1760 MHz): } T_{\text{Rcvr}} &= 8.2 + 0.7(\nu-0.95)/(1.76-0.95) \text{ K} \\ \text{SKA SPF3 (1.65 – 3.05 GHz): } T_{\text{Rcvr}} &= 10.6 + 1.5(\nu-1.65)/(3.05-1.65) \text{ K} \\ \text{SKA SPF4 (2.8 – 5.18 GHz): } T_{\text{Rcvr}} &= 14.3 + 2.4(\nu-2.8)/(5.18-2.8) \text{ K} \\ \text{SKA SPF5 (4.6 – 13.8 GHz): } T_{\text{Rcvr}} &= 16.7 + 6.1(\nu-4.6)/(13.8-4.6) \text{ K} \\ \text{SKA SPF5B (4.6 – 24 GHz): } T_{\text{Rcvr}} &= 17.0 + 6.0(\nu-4.6)/(24.0-4.6) \text{ K} \end{aligned}$$

The effective aperture is given simply by $A_{\text{eff}} = \eta_A A_{\text{Phys}}$, the product of aperture efficiency and physical area. The empirical model for SKA1 aperture efficiency, η_A , and its variation with frequency in GHz, ν , is given by:

$$\eta_A = 0.92 - 70. (\lambda/D)^2 - 0.36 [\text{abs}(\nu-1.6)/(24.0-1.6)]^{0.6}$$

The leading constant is the peak aperture efficiency that is achieved at mid frequencies. The second term describes the reduction in illumination efficiency and diffraction losses at low frequencies while the third term captures losses due to both surface roughness and non-optimum illumination at the highest frequencies.

Current estimates of T_{Rcvr} for each of the MeerKAT SPF bands and their variation with the frequency in GHz, ν , are given by:

$$\begin{aligned} \text{MK UHF (580 – 1020 MHz): } T_{\text{Rcvr}} &= 12. + 0.0(\nu-0.58)/(1.02-0.58) \text{ K} \\ \text{MK L-Band (900 – 1670 MHz): } T_{\text{Rcvr}} &= 10.0 - 2.0(\nu-0.9)/(1.67-0.9) \text{ K} \\ \text{MK S-Band (1.65 – 3.05 GHz): } T_{\text{Rcvr}} &= 10.6 + 1.5(\nu-1.65)/(3.05-1.65) \text{ K} \\ \text{(MK X-Band (8.0 – 14.5 GHz): } T_{\text{Rcvr}} &= 15.0 + 0.0(\nu-8.0)/(14.5-8.0) \text{ K} \end{aligned}$$

The empirical model for MeerKAT aperture efficiency, η_A , and its variation with frequency in GHz, ν , is given by:

$$\eta_A = 0.75 - 70. (\lambda/D)^2 - 0.1 [\text{abs}(\nu-1.6)/(24.0-1.6)]^{0.6}$$

The SKA1-MID deployment calls for 133 SKA1 dishes of 15m diameter providing the sensitivity shown in Figure 1 (in the SPF1, SPF2 and SPF5 bands) as well as integration of the 64 MeerKAT dishes of 13.5m diameter outfitted with UHF, L-Band and S-Band feed systems with the modelled performance figures noted above.

3.2 Sensitivity as function of angular scale for SKA1-MID

To document the variation of sensitivity as a function of angular scale for the SKA1-MID configuration we consider a simulated eight-hour duration tracking observation centred at transit of a source at a nominal declination of -30 deg. For completeness we consider both a monochromatic observation at a single frequency (of 1.4 GHz) as well as a broad-band multi-channel observation that spans 30% fractional bandwidth (0.42 GHz) at this frequency. The same noisy visibilities were then gridded and

imaged with a variety of different data weighting strategies, each on a 2048×2048 pixel grid. A naturally weighted reference image was first made. Subsequently, a sequence of images was formed, each employing a so-called “uniform” weighting of the gridded visibilities followed by a Gaussian tapering to achieve a target Gaussian beamsize. The image cell size was chosen to provide a 4×4 pixel sampling of the target Gaussian FWHM. A logarithmic sampling of Gaussian target beamsizes was undertaken to fully explore the range of scales to which the configuration has any sensitivity. The RMS noise in each of the Gaussian tapered images was compared to the RMS noise in the naturally weighted image. The image noise relative to the natural sensitivity of the entire array is plotted in the bottom panels of Figure 2, as a function of the *actual* measured (rather than the target) FWHM beamsize. Although these simulations have been undertaken at a single frequency, they can simply be shifted linearly to smaller (or larger) beamsizes for higher (or lower) observing frequencies. As seen in the plots, the SKA1-MID configuration provides about 50% of the natural array sensitivity over a very wide range of angular scales. Also shown in the Figures are the near-in (within the central 10×10 FWHM) RMS sidelobe levels of the synthesised beam both for these eight-hour tracks (middle panels) and a single snap-shot at transit (upper panels). At intermediate scales, the dirty beams are extremely well characterised by a Gaussian.

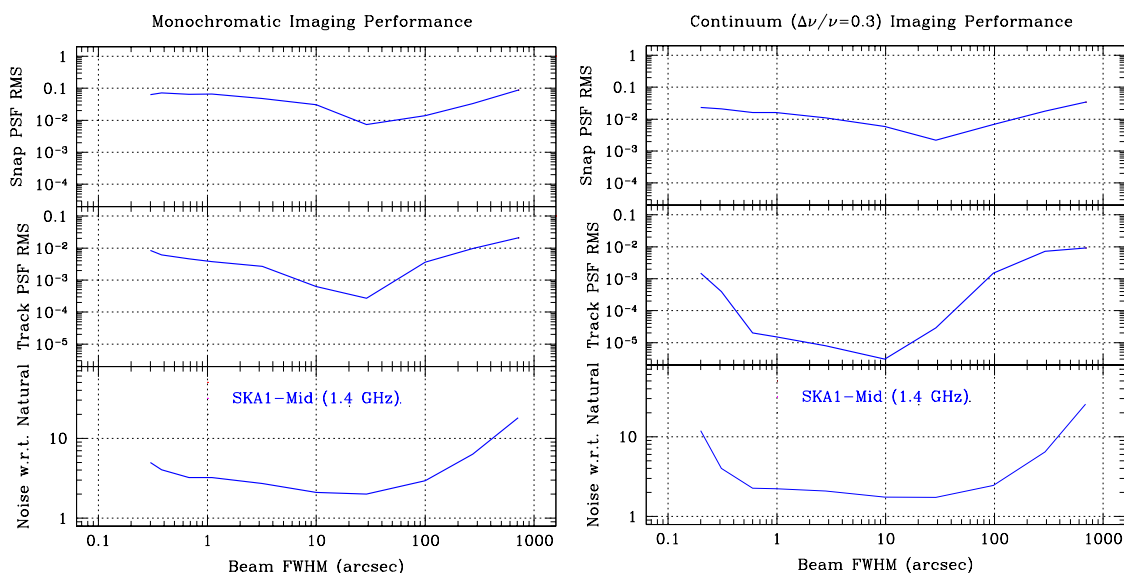


Figure 2. Monochromatic (left) and broad-band (right) image noise and PSF quality performance of the SKA1-MID configuration as function of angular scale.

3.3 Field-of-View of SKA1-MID

Dish primary beam properties depend on the aperture illumination pattern. For an aperture illumination with a 10 dB edge taper of the form $I(r)=1-0.67 r^2$ for $r < 1$, expressed in units of the dish radius, $r_D = D/2$, the resulting power pattern has a FWHM size,

$\theta_{DB} = 66 (\lambda/D)$ degrees, (eg. RD3) and a first sidelobe level of -23 dB. The integral of this power pattern has been evaluated numerically as,

$$\Omega_{DB} = 4320 (\lambda/D)^2 \text{ deg}^2,$$

while the integral of the power pattern squared, the **noise-effective field of view** is,

$$\Omega_{DN} = 2340 (\lambda/D)^2 \text{ deg}^2.$$

This is a good approximation of the field of view for the 15m SKA1 dishes when calculating the Survey Speed.

3.4 Sensitivity of ASKAP

For the current ASKAP MkII PAF design, [RD4] suggest that $T_{\text{sys}}/\eta \approx 80$ K between 1100 and 1300 MHz, climbing to 90K at both lower and higher frequencies as shown in Figure 3. No specific error estimate is given by Chippendale et al., although they quote a minimum uncertainty of 6% due to uncertainty in calibration level. We will make use of the curve given by [RD4] to represent the current ASKAP performance. An estimate of what an ASKAP MkIII PAF might achieve is $T_{\text{sys}}/\eta \approx 50$ K. We will consider both performance scenarios in the comparisons below.

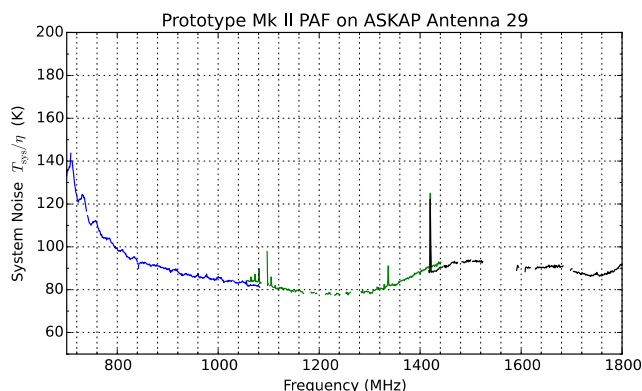


Figure 3. The ratio of system temperature to aperture efficiency T_{sys}/η_A of the ASKAP MkII PAF as published by Chippendale et al. in RD4.

3.5 Sensitivity as function of angular scale for ASKAP

Just as done previously in Section 3.2 for SKA1-MID, the sensitivity as function of angular scale of the ASKAP configuration was determined by simulating eight-hour duration tracking observations at a specific frequency and determining the RMS noise in a sequence of uniformly weighted and Gaussian tapered images relative to a naturally weighted reference image. The relative noise as function of scale is plotted in Figure 4 below. At intermediate scales, the noise is only degraded by about 30% from the natural array sensitivity. However, this is only achieved over a limited range (factor of 2 – 3) in angular scales.

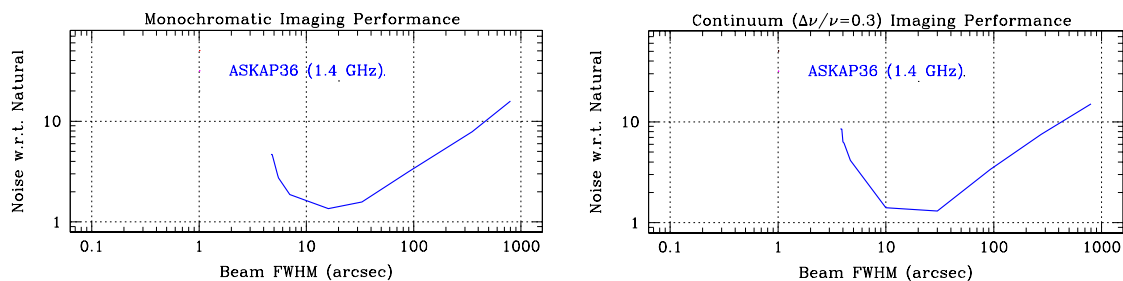


Figure 4. Monochromatic (left) and broad-band (right) image noise of the ASKAP configuration as function of angular scale.

3.6 Field-of-View of ASKAP

For the case of a phased array feed, the noise effective field of view is defined by the integral of the square of the beam-sampled power reception pattern, taking account of the fact that each photon is only counted once despite contributing in some cases to more than one of the digitally combined beams. The integral of the beam-sampled, squared power reception patterns as a function of frequency of the chequerboard PAF design are provided by Hay et al [RD5]. At the highest design frequency of a 36-beam system, the effective PAF FoV approaches 36 times the effective SPF FoV, as shown in Figure 5. At the lowest frequencies of the PAF band ($v_{Max}/2.57$) the effective beam number has declined to about 11 times the effective SPF FoV. The frequency dependence of the noise effective PAF beam number across the band is given for v in the range $v_{Max}/2.57 - v_{Max}$,

$$N_{Bm} = -57.28(v/v_{Max})^2 + 120.4 (v/v_{Max}) - 27.31$$

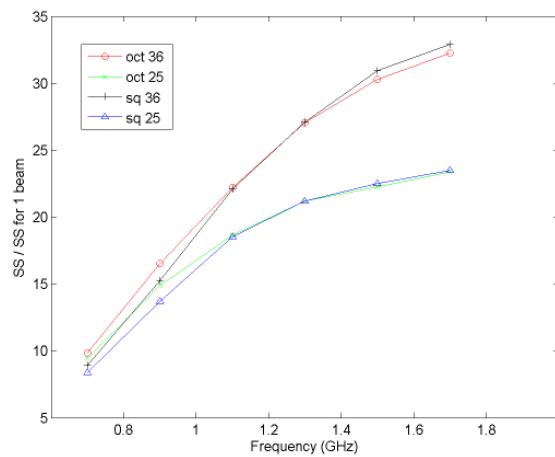


Figure 5. The number of noise effective ASKAP PAF beams as function of frequency as published by Hay et al. in RD5. The “oct36” label refers to the relevant octagonal arrangement of 188 differential ports sampled by 36 digital beams.

The noise effective PAF FoV is just the product of this beam number with the area per beam of a 12m dish, as discussed in Section 3.3 above, $\Omega_{DN} = 2340 (\lambda/D)^2 \text{ deg}^2$.

3.7 Sensitivity and Field-of-View of PAFs on SKA1 dishes

The DSH consortium PDR documentation provided extensive analysis of PAF performance within the SKA1 dish optics as shown in Figure 6. This analysis demonstrated the performance enhancement at low frequencies that is provided by a large secondary reflector (such as has been adopted in the final design) and the lack of performance sensitivity to (non-parabolic) shaping of the primary reflector. The implication is that the same dish design can perform very well with both PAF and SPF systems, so that no design compromise of the basic structure is necessary.

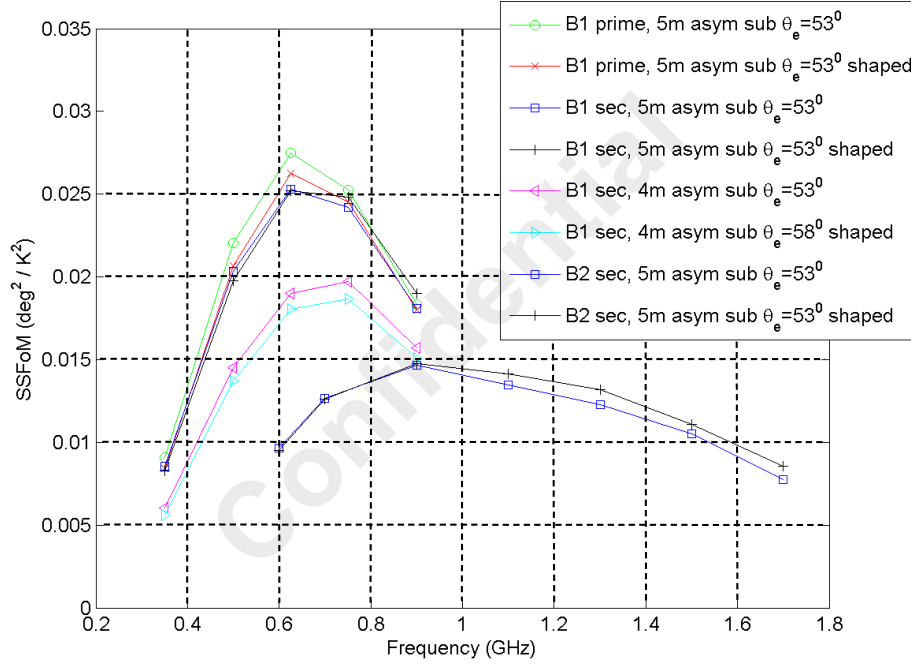


Figure 6. Overview of PAF performance within the SKA1 dish optics as function of frequency as published by Hay & Smith in RD6 assuming an LNA minimum differential noise temperature of 21K. The quantity SSFoM is defined as $FoV (\eta_A/T_{sys})^2$.

We have constructed an empirical model to approximate the results of the EM simulations as follows.

$$T_{Sys} = T_{LNA} + T_{Spill} + T_{Sky}, \text{ where}$$

$$T_{Sky} = T_{Gal} + T_{CMB} + T_{Atm} \text{ following [RD2] with,}$$

$$T_{Gal} = 20 (0.408 \text{ GHz}/\nu)^{2.75} \text{ K,}$$

$$T_{CMB} = 2.73 \text{ K and}$$

$$T_{Atm} = 288 (0.005 + 0.1314 \exp\{8[\log_{10}(\nu) - \log_{10}(22.23 \text{ GHz})]\}) \text{ K}$$

The spill-over component, T_{Spill} , is modelled as a constant in each of the bands,

$$T_{SpillB1} = 6 \text{ K in PAF Band 1 (350 – 900 MHz) and}$$

$$T_{SpillB2} = 4 \text{ K in PAF Band 2 (650 – 1670 MHz). Following Hay & Smith we assume}$$

$$T_{LNA} = 21 \text{ K in both PAF Bands 1 and 2.}$$

The aperture efficiency is modelled as

$$\eta_{AB1} = 0.76 - 45. (\lambda/D)^2 \text{ in PAF Band 1 and,}$$

$$\eta_{AB2} = 0.8 - 45. (\lambda/D)^2 \text{ in PAF Band 2.}$$

The number of noise effective PAF beams is modelled as before with,

$$N_{Bm} = -57.28(\nu/\nu_{Max})^2 + 120.4 (\nu/\nu_{Max}) - 27.31$$

The noise effective PAF FoV is just the product of this beam number with the area per beam of a 15m dish, as discussed in Section 3.3 above, $\Omega_{DN} = 2340 (\lambda/D)^2 \text{ deg}^2$. The empirical model is overlaid on the EM simulations in Figure 7 demonstrating its reasonable agreement.

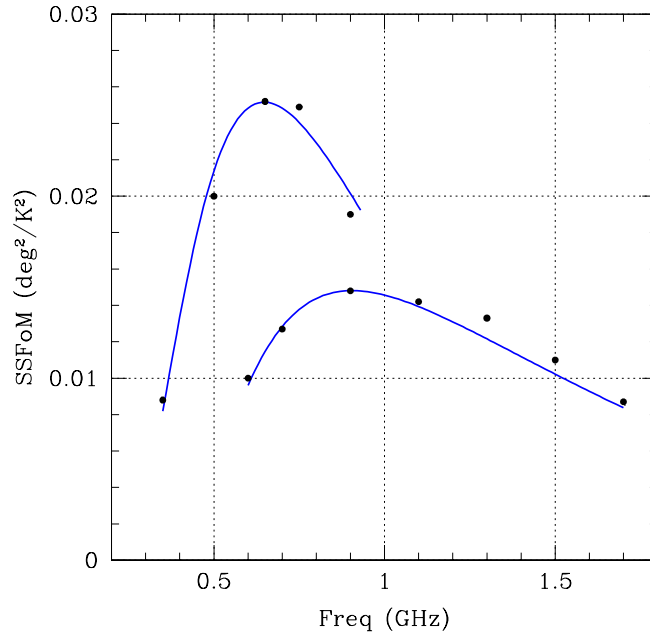


Figure 7. Empirical model of PAF performance within the SKA1 dish optics as function of frequency (blue curves) overlaid on the performance simulations (black points) of Hay & Smith in RD6. The quantity SSFoM is defined as $\text{FoV} (\eta_A/T_{\text{sys}})^2$.

While similar simulations were not presented in [RD6] for the case of PAF Band 3 (1670 – 4000 MHz) we will use the working assumption of $T_{\text{spillB3}} = 4 \text{ K}$, $T_{\text{LNAB3}} = 25 \text{ K}$ and $\eta_{\text{AB3}} = 0.8 - 45 \cdot (\lambda/D)^2$ in PAF Band 3.

4 Survey Speed Comparisons

With knowledge of (a) the natural array sensitivity, (b) the relative sensitivity as function of angular scale and (c) the noise effective field-of-view, all as function of the observing frequency, it is straight forward to produce two dimensional contour plots that document the relative survey speed as function of both angular scale and observing frequency.

4.1 Relative Survey Speed of SKA1-MID and ASKAP MkII

The natural array sensitivity of SKA1–MID is assumed to be that of 133 new 15m SKA1 antennas and the 64 MeerKAT 13.5m antennas with the performance discussed in Section 3.1. The ASKAP array sensitivity is based on 36 antennas of 12m diameter with the noise performance discussed in Section 3.4, based on [RD4]. The ratio of SKA1-MID to ASKAP MkII survey speed is shown in Figure 8. The ratio is only defined where both SKA1-MID and ASKAP have a finite survey speed, so is constrained in both frequency coverage and beam size by the ASKAP capabilities.

As shown in Figure 8, ASKAP survey speed is highest for angular resolutions near 30 arcsec, such as might apply to the unresolved detection of neutral hydrogen emission from red-shifted galaxies. In this regime, the anticipated ASKAP MkII performance is about 14 times lower than SKA1-MID.

For surveys that are targeting broad-band continuum emission, it is vital to achieve an angular

resolution that is significantly higher than 10 arcsec. If this condition is not satisfied, such surveys become limited by what is termed source confusion [RD9], a noise-like fluctuation level that is a consequence of the population of faint unresolved sources within the images. In this regime, the anticipated ASKAP MkII performance is about 30 times lower than SKA1-MID.

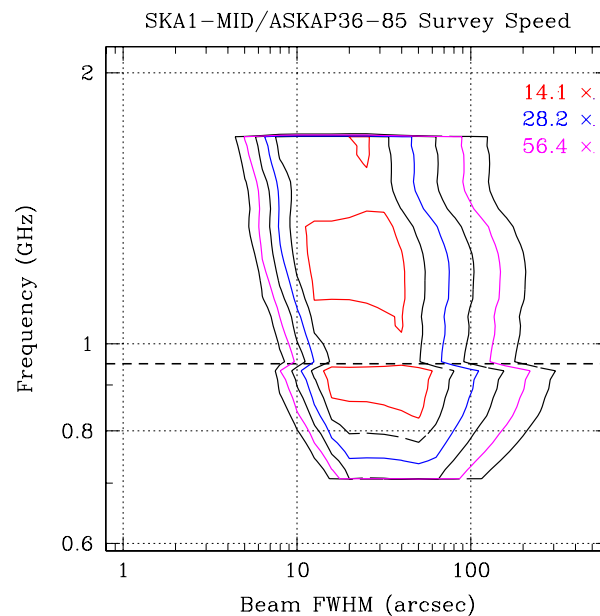


Figure 8. The relative survey speed of SKA1-MID compared to ASKAP equipped with 36 MkII PAFs as function of observing frequency and Gaussian beam size. The ASKAP MkII sensitivity as function of frequency is taken from Chippendale et al [RD4]. The dashed horizontal line marks the boundary between SPF1 and SPF2 for SKA1.

As noted at the outset of Section 3, we have not yet taken into account possible differences in the processed bandwidth, $BW = 800$ (or 700) MHz for SKA1-MID SPF2 (or SPF1) versus $BW = 300$ MHz for ASKAP. Continuum applications would generally benefit in direct proportion to the ratio of processed bandwidth, increasing the survey speed ratios shown in Figure 8 by a factor of about 2.5. For spectral line applications, the survey speed benefit of a larger processed bandwidth would depend on the specific target population and survey strategy, but would generally be less than the simple BW ratio and in those cases that are matched to the smaller ASKAP BW, independent of it.

4.2 Relative Survey Speed of SKA1-MID and ASKAP MkIII

The natural array sensitivity of SKA1-MID is assumed to be that of 133 new 15m SKA1 antennas and the 64 MeerKAT 13.5m antennas with the performance discussed in Section 3.1. The ASKAP array sensitivity is based on 36 antennas of 12m diameter with an assumed noise performance of $T_{\text{sys}}/\eta \approx 50$ K over the full frequency range. The ratio of SKA1-MID to ASKAP MkIII survey speed is shown in Figure 9. The ratio is only defined where both SKA1-MID and ASKAP have a finite survey speed, so is constrained in both frequency coverage and beam size by the ASKAP capabilities.

As shown in Figure 9, ASKAP survey speed is highest for angular resolutions near 30 arcsec, such as might apply to the unresolved detection of neutral hydrogen emission from red-shifted galaxies. In this regime, the anticipated ASKAP MkII performance is about 5 times lower than SKA1-MID.

For surveys that are targeting broad-band continuum emission, it is vital to achieve an angular resolution that is significantly higher than 10 arcsec. If this condition is not satisfied, such surveys become limited by what is termed source confusion, a noise-like fluctuation level that is a consequence of the population of faint unresolved sources within the images. In this regime, the anticipated ASKAP MkII performance is about 10 times lower than SKA1-MID.

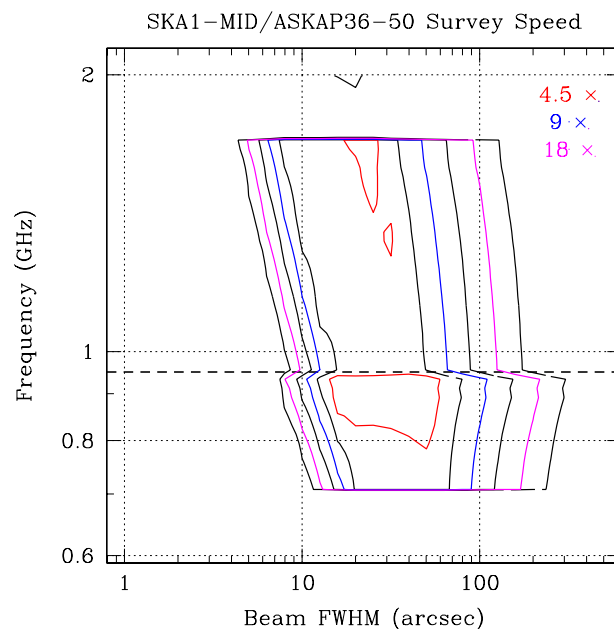


Figure 9. The relative survey speed of SKA1-MID compared to ASKAP equipped with 36 MkIII PAFs as function of observing frequency and Gaussian beam size. The ASKAP MkIII sensitivity as assumed to be $T_{\text{sys}}/\eta \approx 50$ K over the full frequency range. The dashed horizontal line marks the boundary between SPF1 and SPF2 for SKA1.

As noted above, we have not yet taken into account possible differences in the processed bandwidth, $BW = 800$ (or 700) MHz for SKA1-MID SPF2 (or SPF1) versus $BW = 300$ MHz for the *current* ASKAP system. Continuum applications would generally benefit in direct proportion to the ratio of processed bandwidth, increasing the survey speed ratios shown in Figure 9 by a factor of about 2.5. For spectral line applications, the survey speed benefit of a larger processed bandwidth would depend on the specific target population and survey strategy, but would generally be less than the simple BW ratio and in those cases that are matched to the smaller ASKAP BW, independent of it.

4.3 Relative Survey Speed of SKA1 dishes with SPFs and PAFs

It is interesting to consider the relative survey speed of SKA dishes when outfitted with PAFs relative to SPFs. In this case it is sufficient to compare the performance of an individual dish or collection of dishes, rather than considering distinct array configurations. The noise and FoV performance of the PAF and SPF systems have been documented in Sections 3.1, 3.3 and 3.7 above. The relative survey speed as function of frequency is shown in Figure 10. The frequency ranges of the individual feed systems are marked with vertical dashed lines in red for the PAFs and in magenta for the SPFs.

For the frequency range covered by SPF2 the survey speed increase enabled by a PAF deployment varies between about 5 to 7 across the band. Within the frequency range covered by SPF3 this varies

from 4 to 10. The largest survey speed enhancements are achieved in the frequency range covered by SPF1, where they vary between 10 and 15, and indeed SPF4 and above. Significant PAF design effort within the SKA DSH consortium was focused on the PAF1 and PAF2 bands, rather than on development of higher frequency PAFs.

From this comparison it would appear that the greatest scientific return of a PAF deployment might be realised with the PAF1 band providing enhanced access to many cosmological probes (red-shifted HI, high densities of continuum sources, etc.) below about 1 GHz. Substantial gains in survey speed might also be realised in the longer term from development and deployment of high frequency PAFs (covering 3 GHz and above).

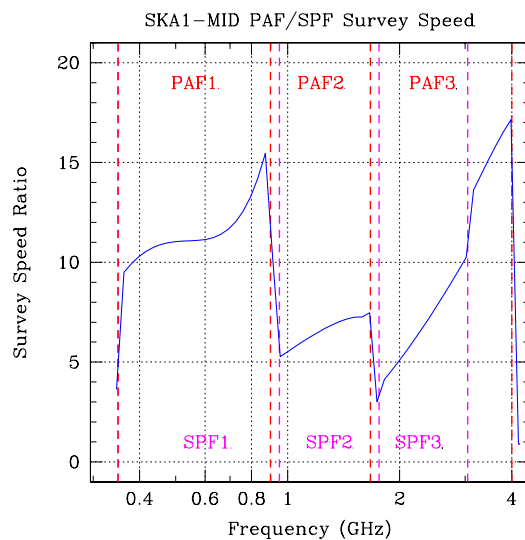


Figure 10. The relative survey speed of SKA1 dishes when equipped with PAFs versus SPFs.